Journal of Sound and Vibration (2001) **246**(4), 705–721
doi:10.1006/jsvi.2001.3695, available online at http://www.idealibrary.com on IDEAL®

UNSTEADY DRAG ON A CYLINDER DUE TO TRANSVERSE OSCILLATION AT FINITE AMPLITUDE

C. L. MORFEY

Institute of Sound and Vibration Research, University of Southampton, Southampton SO17 1BJ, England. E-mail: clm@isvr.soton.ac.uk

AND

M. TAN

School of Engineering Sciences (Ship Science), University of Southampton, Southampton SO17 1BJ, England

(*Received* 8 *September* 2000, *and in final form* 19 *March* 2001)

Transverse oscillations of a cylinder in a viscous fluid generate a force on the fluid that becomes non-linear at large oscillation amplitudes. When the cylinder motion is sinusoidal, non-linearity produces odd order harmonic distortion in the force. Numerical simulations based on the incompressible Navier–Stokes equations are used to explore (1) departures from linear theory and (2) the approach to quasi-steady behaviour, for oscillations over a wide frequency range at peak Reynolds numbers between 10^{-2} and 10. Non-linearity appears once the displacement amplitude becomes comparable with the viscous penetration depth at the oscillation frequency. The results provide insight into the attenuation of sound in air-filled fibrous materials, where non-linear behaviour has been observed at sound pressure levels around 150 dB and upwards (see the paper by H.L. Kuntz and D.T. Blackstock 1987 *Journal of the Acoustical Society of America* **81**, 1723–1731 [3]).

1. INTRODUCTION

A long circular cylinder oscillating transversely in a viscous fluid at rest applies an unsteady force to the fluid. A similar situation occurs when a fixed cylinder is placed in a plane-wave sound field, with its axis normal to the propagation direction. Provided the cylinder diameter, d, is small compared with the acoustic wavelength at the oscillation frequency, the forces in the two situations are closely related (as described in section 1.1), and can be calculated analytically in the small-amplitude limit [1, 2; see also Appendix A].

However, non-linear phenomena—including streaming and, eventually, turbulence—begin to influence the unsteady drag as the oscillation amplitude is increased. In this paper, a numerical boundary element method will be used to explore the onset of non-linearity for a sinusoidally oscillating cylinder, under conditions of laminar flow.

1.1. BACKGROUND AND MOTIVATION

Apart from its fundamental interest as an unsolved problem in fluid flow, the question of when and how the linear drag approximation breaks down has a practical motivation in acoustics, since the attenuation of sound by fibrous absorbing materials is known to

0022-460X/01/390705 + 17 $35.00/0

become non-linear at large amplitudes [3, 4]: this typically occurs at sound pressure levels in air above 150 dB $re(20\,\mu\text{Pa})^2$. Non-linearity of the hydrodynamic force on a single cylindrical fibre is an obvious mechanism of non-linear attenuation.

The parameter range of the present study matches typical sound-absorption applications. It is confined to low Reynolds numbers ($R \leqslant 10$), where R is the oscillatory Reynolds number based on the peak velocity v_{max}:

$$R = \frac{\rho v_{max} d}{\mu} \quad (\rho = \text{fluid density}, \mu = \text{viscosity}). \tag{1}$$

The frequency range is limited to low Stokes numbers based on cylinder diameter ($S \lesssim 3$):

$$S = \frac{\rho \omega d^2}{\mu} = 2\left(\frac{d}{\delta}\right)^2 \quad (\text{angular frequency } \omega = 2\pi f;\ \delta = \sqrt{2\nu/\omega};\ \nu = \mu/\rho). \tag{2}$$

For a cylinder of diameter 15 μm in air (at 15°C, 1 atm), $R = 1$ corresponds to a velocity amplitude of 1 m/s, while $S = 1$ corresponds to an oscillation frequency of 10 kHz. One outcome of the study is that as S is increased with R held constant, the fluid loading moves closer to linear theory (as will be demonstrated below).

In what follows, the cylinder is assumed to oscillate with velocity $v(t)$ is a *stationary* viscous fluid of infinite extent. The fluid is modelled as incompressible, which means that the results apply in the combined limit of low Mach number ($v_{max}/c \ll 1$, where v_{max} is the peak velocity and c is the speed of sound) and low Helmholtz number ($\omega d/c = 2\pi d/\lambda \ll 1$). Once the unsteady drag is known for this case, it can easily be generalized to the case of a cylinder in a uniformly accelerating fluid, by using the equivalence relation for incompressible flow [5]. This states that the relative flow field around any rigid body moving with velocity $\mathbf{V}(t)$, in a time-varying uniform stream whose velocity at infinity is $\mathbf{U}(t)$, is identical at every instant to the flow field around the same body as it moves with velocity $\mathbf{V}(t) - \mathbf{U}(t)$ through the same fluid at rest. The unsteady forces $\mathbf{F}_{\mathbf{U}}(t)$, $\mathbf{F}_0(t)$ exerted by the body on the fluid in the two cases are related by

$$\mathbf{F}_{\mathbf{U}}(t) = \mathbf{F}_0(t) - m_{displ}\dot{\mathbf{U}}(t), \tag{3}$$

where m_{displ} is the mass of fluid that the body displaces and $\dot{\mathbf{U}}(t)$ is the fluid acceleration at infinity. Note that because the correction term is linear in $\mathbf{U}(t)$, it makes no contribution to the non-linear drag effects discussed below. A list of nomenclature is given in Appendix D.

1.2. COMPARISONS AVAILABLE FROM PREVIOUS STUDIES

The two-dimensional flow round a circular cylinder oscillating transversely in a viscous incompressible fluid can be solved exactly in two limiting cases: (1) oscillations of small amplitude, defined by the limit $R \to 0$, with S fixed: here the drag is given by linearized theory as described in Appendix A; (2) oscillations at finite but low Reynolds numbers ($R < 10$), in the low-frequency limit defined by $S \to 0$, with R fixed; here inertial effects are small, and the flow is *quasi-steady* relative to the cylinder. The known solutions for the drag in these two cases are used in section 3 as benchmarks, in order to validate the numerical results obtained for finite (R, S).

An important objective is to explore under what circumstances each of these limiting solutions provides a good approximation to the drag. The answers are given for case (1) in section 3.2, and for case (2) in section 3.3. It turns out that the respective domains of

approximate validity, expressed in a suitable non-dimensional parameter space, have no overlap. For a fixed Reynolds number, the linear solution is approached in the *high-frequency* limit, and the quasi-steady solution is approached in the *low-frequency* limit.

Our literature research revealed no published experiments or numerical studies on cylinder drag whose parameter ranges overlap with the present investigation. However, extensive experimental and numerical work has been done [6, 7] on the special case $d \to \infty$ (or in dimensionless terms, $S \to \infty$), which corresponds locally to an infinite flat plate oscillating in its own plane next to a semi-infinite viscous fluid. Flat-plate experiments, using single-frequency excitation, show that the oscillatory flow remains laminar as long as the peak boundary displacement ξ_{max} does not exceed 250δ. Transition to turbulence—in the form of transient turbulent bursts, that develop explosively during the deceleration phase of each cycle and disappear during the acceleration phase—has been observed to occur in the flat-plate Stokes boundary layer within the range of amplitudes

$$250 < \xi_{max}/\delta < 285 \quad \text{(equivalent to } 500 < v_{max}\delta/\nu < 570\text{)}. \tag{4}$$

In terms of the parameters R and S for flow around an oscillating cylinder, equation (4) means that turbulent transition in the large-S (or flat-plate) limit occurs in the range

$$0{\cdot}13 \times 10^4 < R^2/S < 0{\cdot}16 \times 10^4. \tag{5}$$

Despite the very different Stokes number range of the present study ($S \lesssim 3$, as opposed to $S \to \infty$), the same parameter R^2/S ($= \rho {v_{max}}^2/\omega\mu$) will be shown to be significant for the present oscillating-cylinder problem—not in determining transition, but in determining the onset of non-linearity.

Finally, a review by Wang [8] of work prior to 1968 noted that in the laminar regime, non-linear corrections to the linear flow solution can be calculated by asymptotic methods for $R^2/S \ll 1$, but that such corrections are typically limited to a small part of the (R, S) parameter space†. Published solutions are mostly directed at the steady streaming component; the only non-linear corrections available for the oscillatory-drag problem are for $S \gg 1$ (where an oscillatory boundary layer exists around the cylinder; results for this case are given in reference [8]). The method of successive approximations, used by Holtsmark *et al.* [9] to investigate streaming for arbitrary S, could be used to give the drag; but for that purpose it would need to be carried at least to third order in the amplitude. Unfortunately, the study by Holtsmark *et al.* [9] stops at the second order approximation.

2. DIMENSIONLESS PARAMETERS AND SCALING

For maximum generality, dimensionless variables are used in this study. The instantaneous force $f(t)$ per unit length exerted by an infinite cylinder on the surrounding fluid, when the cylinder oscillates transversely at angular frequency ω with peak velocity v_{max}, depends on the parameters (v_{max}, ω, μ, ρ, d). Since $f(t)$ is expected to scale linearly on v_{max} at small amplitudes, it is convenient to normalize the instantaneous force as follows:

$$\frac{f(t)}{v_{max}} = \phi(t, v_{max}, \omega, \mu, \rho, d). \tag{6}$$

† Note that our parameters (R, S) are denoted by the symbols (R, RS) in reference [8]. Wang's symbol S (for Strouhal number) corresponds to our $1/K$, where K is the amplitude parameter introduced in equation (8).

Here ϕ is an unknown periodic function, to be determined numerically. Expressing equation (6) in dimensionless form requires four dimensionless groups, one of which is chosen as $f(t)/\mu v_{max}$. Fourier analysis with respect to τ, the dimensionless time measured in cycles, then yields

$$\frac{f(t)}{\mu v_{max}} = \mathrm{Re}\{H_1 e^{j2\pi\tau} + H_2 e^{j4\pi\tau} + \cdots\} = \mathrm{Re}\left\{\sum_{n=1}^{\infty} H_n e^{j2n\pi\tau}\right\}; \tag{7}$$

the phase and amplitude of each force harmonic are described here by the complex coefficients H_n.

The dimensionless force coefficients $H_n (n = 1, 2, 3, \ldots)$ depend on two dimensionless parameters,‡ which are chosen as S and $K (= R/S)$. Both have a physical interpretation. The parameter K, given by

$$K = \frac{v_{max}}{\omega d}, \tag{8}$$

is the ratio of the oscillation amplitude to the cylinder diameter; $2\pi K$ is sometimes called the Keulegan–Carpenter number. The frequency parameter S is a measure of the cylinder diameter in terms of the Stokes layer thickness δ; from equation (2),

$$S = 2(d/\delta)^2, \qquad \delta = \sqrt{2\nu/\omega} \quad (\nu = \text{kinematic viscosity } \mu/\rho). \tag{9}$$

When S is much greater than 1, the Stokes layer is thin on the scale of the cylinder diameter, and boundary-layer approximations are appropriate. However, it will be shown that over the entire Reynolds number range $0{\cdot}01 \leqslant R \leqslant 10$, the cylinder drag becomes significantly non-linear only at low frequencies such that S is less than R^2. The non-linear phenomena of this paper therefore lie outside the scope of boundary-layer theory.

3. NUMERICAL RESULTS FOR OSCILLATORY DRAG

3.1. SCOPE OF THE NUMERICAL STUDY

Figure 1 shows the region of K–S space investigated. It is bounded by the diagonal lines marked $R = 10$ and $0{\cdot}01$ on the log–log plot; these are the upper and lower Reynolds number limits.

At each of the 26 numbered points in Figure 1, the simulated flow was run to a steady state as described in Appendix B (where a brief account of the numerical method may be found). In a post-processing operation, the dimensionless force harmonics H_n defined in equation (7)—with magnitudes h_n—were extracted from the final cycle of force data. Points 0–21 were filled in progressively, the main criterion being to cover the region of significant non-linearity. Four extra points (numbered 22–25) were added in the bottom right corner, to provide a comparison with the quasi-steady approximation.

Note that symmetry requires that the even force harmonics be zero, in the absence of a bias flow. (Although one can imagine symmetry being broken at high Reynolds numbers by the onset of chaos, or by sensitivity to initial conditions, such behaviour is not expected

‡ Note that allowing the fluid to be compressible would require introduction of a further parameter, such as the Helmholtz number N or alternatively the Mach number $M = KN$. However, provided $M \ll 1$ as well as $N \ll 1$, the incompressible model provides a good approximation for acoustical purposes (as noted in section 1.1).

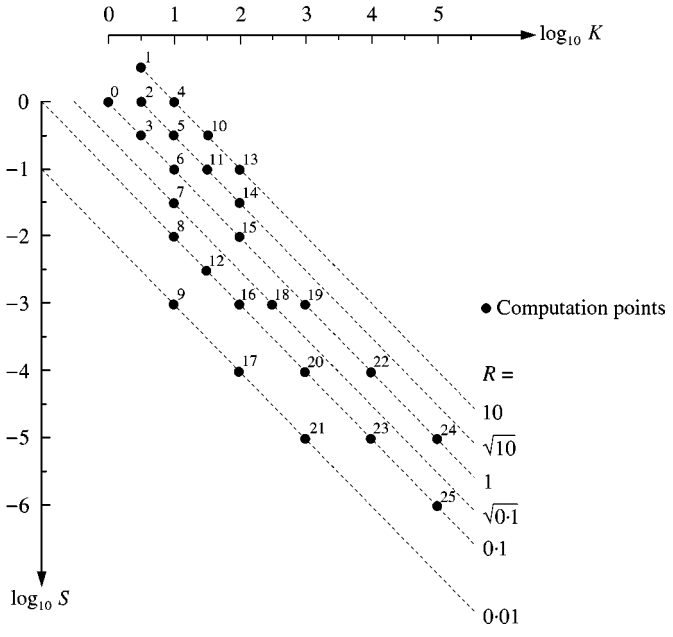

Figure 1. The combinations of amplitude parameter K and dimensionless frequency S used in the computational study. Diagonal lines correspond to fixed values of R, the peak oscillatory Reynolds number.

for $R \leqslant 10$ and was not observed.) Departures from linearity are examined in section 3.2, and convergence with linear theory is demonstrated as K is reduced for constant S. Section 3.3 is focused on departures from quasi-steady drag behaviour, and demonstrates convergence with quasi-steady predictions as S is reduced for fixed R; the convergence criterion is interpreted physically in section 3.4. Finally, a summary of numerical results is presented in section 3.5 for the odd-harmonic amplitudes h_n ($n = 1$–7). An approximate collapse of the harmonic-distortion amplitudes, covering the range $0{\cdot}01 \leqslant R \leqslant 10$, is demonstrated by plotting against the parameter R^2/S.

3.2. CONVERGENCE WITH LINEAR THEORY IN THE SMALL-AMPLITUDE LIMIT

As an illustration of how the computed h_1 value approaches linear theory as the amplitude parameter K is reduced, Figure 2 shows h_1 plotted versus K for a fixed S of 10^{-3}; the linear-theory prediction is shown by the broken line. Convergence of the full numerical result with the analytical prediction provides evidence that the code is working correctly; the difference is less than 1·5 parts per thousand at $K = 10$ (i.e., at point 9 in Figure 1). At the other extreme ($K = 1000$, corresponding to $R = 1$), h_1 is almost twice its linear value. The onset of non-linearity between $K = 10$ and 100 is apparent in this plot.

An alternative presentation of the same data appears in Figure 3. Here the focus is placed on *departures* from the linear analytical solution h_a, by plotting the difference $|h_1 - h_a|$ on a logarithmic scale. The accompanying panels show the higher odd harmonics (3, 5, and 7), for which linearized theory gives zero amplitude.

Note the numerical "noise floor" that appears in the fifth and seventh harmonic results for small K; this limits the dynamic range to a factor of 10^6, meaning that h_n values smaller than $10^{-6}h_1$ are beyond the reach of the present calculation. There is also evidence in Figure 3 of higher-harmonic saturation at large amplitudes.

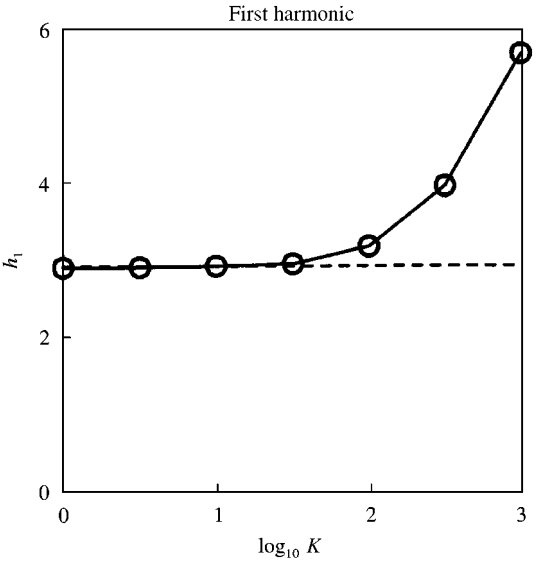

Figure 2. Comparison between the non-linear boundary element method and the linearized analytical solution, for the fundamental amplitude of the dimensionless force at Stokes number $S = 10^{-3}$: O, computed values, domain terms not included; ------, analytical solution.

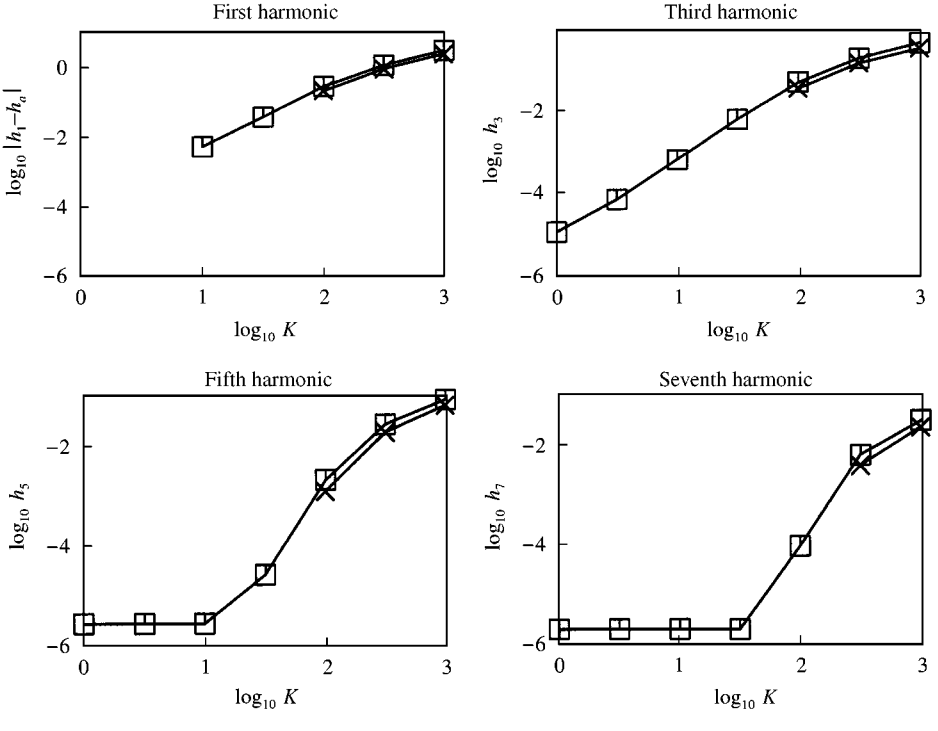

Figure 3. Departures from the linearized solution for the oscillatory force, plotted as a function of the amplitude parameter K for Stokes number $S = 10^{-3}$: ×, full non-linear solution; □, solution without domain terms.

3.3. CONVERGENCE WITH STEADY FLOW IN THE LOW-FREQUENCY LIMIT

The drag coefficient for steady incompressible flow past a circular cylinder has previously been computed [10] over a range of Reynolds numbers of order 1, using the same BEM code described in Appendix B. The results converge to the analytical Oseen solution of Tomotika and Aoi [11, 12] in the limit $R_{mean} \to 0$, where $R_{mean} = Ud/\nu$ is the *steady-flow* Reynolds number. The cylinder drag coefficient, defined as

$$C_D(R_{mean}) = f/(\tfrac{1}{2}\rho U^2 d) \quad (f = \text{drag/unit length; } v = \text{relative velocity}), \tag{10}$$

is given in reference [10] as

$$C_D(R_{mean}) = \left(\frac{8\pi}{R_{mean}}\right)\frac{1 - 0{\cdot}036\sigma + 0{\cdot}303\sigma \ln \sigma}{\mathrm{I}_0(\sigma)\mathrm{K}_0(\sigma) + \mathrm{I}_1(\sigma)\mathrm{K}_1(\sigma)}, \tag{11}$$

where σ equals $R_{mean}/4$. The factor $(8\pi/R_{mean})(\mathrm{I}_0\mathrm{K}_0 + \mathrm{I}_1\mathrm{K}_1)^{-1}$ above, involving the modified Bessel functions I and K, is the asymptotic result [11, 12] for $R_{mean} \ll 1$; the remaining factor is a residual correction for finite R_{mean}, obtained from steady-flow numerical calculations for $R_{mean} = 0{\cdot}1\ (0{\cdot}1)1{\cdot}0$ by curve-fitting.

As the oscillation frequency is reduced, the flow round the oscillating cylinder is expected to become quasi-steady. Specifically, in the limit defined by $S \to 0$, with $KS = R$ held constant, the instantaneous force corresponding to a cylinder velocity $v_{max}\cos\omega t$ should follow the steady-flow relation at every instant:

$$f(t) = \tfrac{1}{2}\,\rho\, {v_{max}}^2\, d\, C_D(R\cos\omega t)\cos^2\omega t, \tag{12}$$

or in dimensionless form

$$\frac{f(\tau)}{\mu v_{max}} = \frac{1}{2}\, R\, C_D(R\cos 2\pi\tau)\cos^2 2\pi\tau. \tag{13}$$

By using equation (11) for C_D and evaluating equation (13) over a complete cycle, the dimensionless drag harmonic amplitudes h_n can be found in the quasi-steady limit. Figure 4 shows how each of the computed harmonic amplitudes h_n ($n = 1, 3, 5, 7$) converges to its long-period limiting value $h_{n\infty}$. The ratios $h_n/h_{n\infty}$ are plotted versus S, for $R = 0{\cdot}1$ and 1; in the limit $S \to 0$, $h_n/h_{n\infty}$ tends towards unity. This agreement provides a second benchmark check on the BEM code. Convergence within 5% for h_1 appears to require $S/R^2 < 10^{-4}$, or equivalently $K^2S > 10^4$.

3.4. PHYSICAL INTERPRETATION OF THE QUASI-STEADY DRAG CRITERION

One can express the criterion $K^2S > 10^4$ as follows, with ξ_{max} used to denote the amplitude of the cylinder displacement and δ denoting the viscous diffusion length scale $\sqrt{2\nu/\omega}$:

$$\xi_{max} > 70\delta, \quad \text{or equivalently } \delta > \frac{140}{R}\, d. \tag{14}$$

This dimensional version of the quasi-steady drag criterion has clear physical implications. When K^2S exceeds 10^4, the cylinder displacement ξ_{max} is much greater than the diffusion length δ, and the diffusion length (for $R \leqslant 10$) is much greater than the cylinder diameter d. Under these conditions, convection of vorticity relative to the cylinder is far more powerful

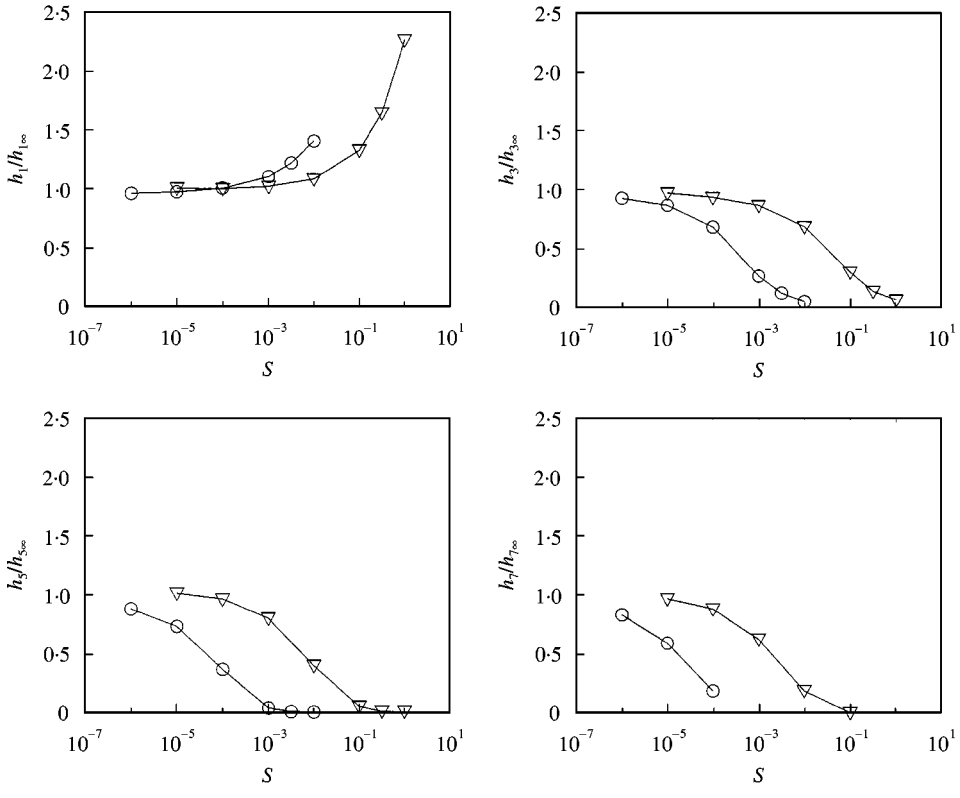

Figure 4. Demonstration of the approach of odd-harmonic force amplitudes to their quasi-steady limiting values, as S tends to zero for fixed R: $\bigtriangledown$, $R = 1$; $\bigcirc$, $R = 0{\cdot}1$.

than vorticity diffusion. Once vorticity has been generated by viscous action close to the cylinder, it is quickly swept many diameters downstream, and the past history of the flow is forgotten within a small fraction of one oscillation period.[§] If follows that the instantaneous force applied to the fluid is virtually the same at every instant as if the cylinder were in *steady* motion.

3.5. SUMMARY OF NUMERICAL RESULTS FOR UNSTEADY DRAG

Table 1 presents harmonic-amplitude data h_n ($n = 1, 3, 5, 7$) for all the (K, S) combinations shown in Figure 1. Also shown are h_1 from linear theory, denoted by h_a, and the difference $|h_1 - h_a|$. Note that in the quasi-steady limit ($S \to 0$), h_a tends to zero (as can be verified from Appendix A).

3.5.1. *Empirical collapse of non-linear harmonic amplitudes*

A quantitative measure of the drag non-linearity is provided by the following dimensionless ratios:

$$\text{(Fundamental)} \quad |h_1 - h_a|/h_a = \varepsilon_1; \quad \text{(higher harmonics, } n > 1\text{)} \quad h_n/h_a. \tag{15}$$

[§]The time scale on which the influence of the convected vorticity disappears is of order $2\pi d/v_{max}$. This represents a fraction $1/K$ of a cycle, which is necessarily a small number (less than 10^{-3}) since $K^2S > 10^4$ and $KS \leqslant 10$.

TABLE 1

Dimensionless harmonic amplitudes of the cylinder force. For each of the points in Figure 1, *the dimensionless amplitudes* h_1, h_3, h_5, h_7 *were computed directly using the BEM code*; *blank entries arise where the harmonic component was too small relative to the numerical noise to allow an accurate determination. For the quasi-steady calculations at* $R = 1{\cdot}0$ *and* $0{\cdot}1$, *dimensionless harmonic amplitudes were obtained by Fourier analysis of the force–time history calculated from equations* (11) *and* (13).

Point	$\log_{10} K$	$\log_{10} S$	R	h_a	$\lvert h_1 - h_a \rvert$	h_1	h_3	h_5	h_7
Parametric study data									
0	0·0	+0·0	1·0	11·072	0·1308	11·203	0·0261	0·0001	—
1	0·5	+ 0·5	10·0	17·153	4·7861	21·939	0·8480	0·0870	0·0083
2	0·5	+ 0·0	$\sqrt{10}$	11·072	1·3230	12·395	0·2271	0·0085	0·0003
3	0·5	− 0·5	1·0	7·8265	0·3263	8·1528	0·0529	0·0007	—
4	1·0	+ 0·0	10·0	11·072	6·3421	17·414	0·9770	0·1527	0·0412
5	1·0	− 0·5	$\sqrt{10}$	7·8265	2·1513	9·9778	0·3470	0·0269	0·0051
6	1·0	− 1·0	1·0	5·9287	0·6604	6·5891	0·1124	0·0038	0·0001
7	1·0	− 1·5	$\sqrt{0{\cdot}1}$	4·7272	0·1700	4·8972	0·0279	0·0003	—
8	1·0	− 2·0	0·1	3·9139	0·0367	3·9506	0·0070	0·0001	—
9	1·0	− 3·0	0·01	2·8989	0·0035	2·8954	0·0005	—	—
10	1·5	− 0·5	10·0	7·8265	7·6306	15·457	1·2509	0·1162	0·0422
11	1·5	− 1·0	$\sqrt{10}$	5·9287	2·9825	8·9112	0·5222	0·0542	0·0070
12	1·5	− 2·5	0·1	3·3328	0·0944	3·4272	0·0159	0·0002	—
13	2·0	− 1·0	10·0	5·9287	8·5106	14·439	1·3748	0·2193	0·0650
14	2·0	− 1·5	$\sqrt{10}$	4·7272	3·5841	8·3113	0·5865	0·0939	0·0026
15	2·0	− 2·0	1·0	3·9139	1·4567	5·3706	0·2531	0·0305	0·0061
16	2·0	− 3·0	0·1	2·8989	0·2006	3·0995	0·0343	0·0012	—
17	2·0	− 4·0	0·01	2·2969	0·0154	2·3123	0·0027	—	—
18	2·5	− 3·0	$\sqrt{0{\cdot}1}$	2·8989	0·8221	3·7210	0·1402	0·0177	0·0035
19	3·0	− 3·0	1·0	2·8989	2·1595	5·0584	0·3196	0·0614	0·0205
20	3·0	− 4·0	0·1	2·2969	0·5249	2·8218	0·0867	0·0119	0·0027
21	3·0	− 5·0	0·01	1·9004	0·1018	2·0022	0·0158	0·0006	0·0001
22	4·0	− 4·0	1·0	2·2969	2·6628	4·9597	0·3443	0·0737	0·0289
23	4·0	− 5·0	0·1	1·9004	0·8312	2·7316	0·1102	0·0239	0·0086
24	5·0	− 5·0	1·0	1·9004	3·0724	4·9728	0·3571	0·0774	0·0317
25	5·0	− 6·0	0·1	1·6201	1·0789	2·6990	0·1178	0·0287	0·0121
Quasi-steady state data									
—	—	—	0·1	—	—	2·7982	0·1264	0·0328	0·0146
—	—	—	1·0	—	—	4·9350	0·3653	0·0769	0·0329

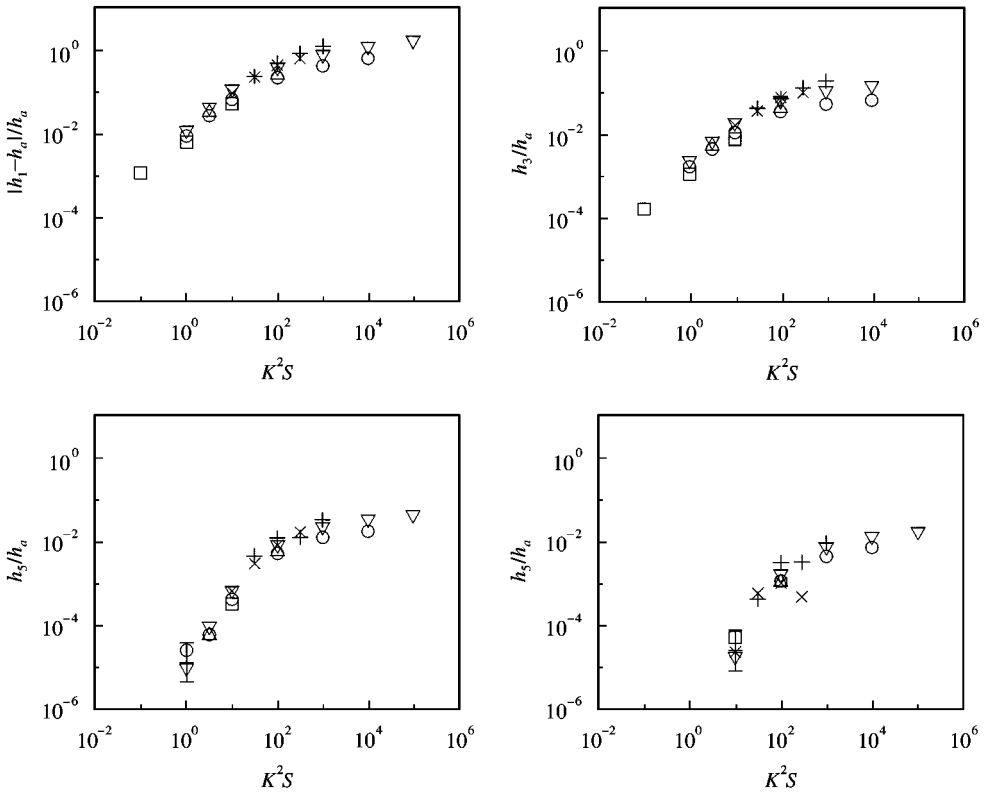

Figure 5. Harmonic-distortion amplitudes normalized on the fundamental amplitude h_a from linearized theory, showing how the data for all the available (K, S) combinations tend to collapse as a function of K^2S: $+$, $R = 10$; $\times$, $R = \sqrt{10}$; $\triangledown$, $R = 1$; $\triangle$, $R = \sqrt{0{\cdot}1}$; $\bigcirc$, $R = 0{\cdot}1$; $\square$, $R = 0{\cdot}01$.

The data in Table 1 show a monotonic increase in these ratios as K increases, for a given S; what is less obvious, until the data are plotted as in Figure 5, is that they tend to collapse on the parameter K^2S. Different symbols in Figure 5 label different Reynolds numbers R; note that all the data points in Figure 1 are included in the plots, except where the harmonic amplitude was too small to resolve numerically. Although the collapse is not perfect, it offers a useful guide to the frequency-dependent onset of non-linearity, in the drag of a sinusoidally oscillating cylinder at peak Reynolds numbers between 0·01 and 10.

3.5.2. *Asymptotic power laws in the low-amplitude limit*

Based on the theoretical studies of Wang [8] and Holtsmark *et al.* [9], together with the directional symmetry of the present problem (which eliminates even harmonics), one might conjecture the asymptotic amplitude dependence of each force harmonic to be of the form

$$f_n \propto K^n + O(K^{n+2}) \quad (n = 1, 3, 5, \ldots), \tag{16}$$

as K tends to zero with S fixed. This would imply $h_n \sim K^{n-1}$ for $n \geqslant 3$, and $|h_1 - h_a| \sim K^2$. The data in Table 1 do not cover sufficient dynamic range to test this hypothesis, because of the noise floor already mentioned; however, that the h_3 results for $S = 10^{-3}$ (points 9, 16, 18, 19 in Figure 1) clearly show a tendency to approach the expected asymptotic K^2 dependence for small K, and there is a similar tendency in the $|h_1 - h_a|$ results. Figure 5 provides further support, in panels 1–3.

4. APPLICATION TO NON-LINEAR SOUND ATTENUATION IN A FIBRE BLANKET

The propagation of small-amplitude sound waves transverse to the fibre direction in a fluid-saturated fibre blanket can be described, in the high-porosity limit, by the model outlined in Appendix C. Here the individual fibres are replaced by sources of heat and momentum distributed in the surrounding fluid. In order to quantify the exchange of heat and momentum between the fibre skeleton and the fluid, each fibre is represented as an isolated cylinder of infinite length; the background 2-D temperature and velocity fields around each fibre are those associated with sound propagation in the blanket, and are equated to the spatially averaged fluid temperature and velocity over a region containing several fibres.

The drag non-linearity described in section 3 can be included in an *ad hoc* way in this linear propagation model, by applying a factor $(1 + \varepsilon_1)$ to the linear drag impedance, z_f, for a single fibre as given in equation (C7). Both the dimensionless impedance, Z_{rel}, and the increase in attenuation coefficient, $\Delta\alpha$, can be estimated in this way, for the fundamental frequency component of an initially sinusoidal plane acoustic wave propagating in the blanket at high intensity. Note that Z_{rel} is required in order to convert the velocity amplitude parameter K into a sound pressure level in the blanket; typically, $|Z_{rel}|$ varies between 1·2 and 2·5, for the air-filled blanket modelled in reference [13].

This approach has been used by the first author [13] to interpret the experimental data of Kuntz and Blackstock [3], for plane-wave propagation in a batted Kelvar®29 air-filled fibre blanket (fibre diameter 12 μm, porosity 0·980). The low-amplitude measurements of phase speed and attenuation in reference [3] were quite well predicted by the linear model between 500 Hz and 2 kHz. When the non-linear correction procedure described above was applied, the predicted increase in attenuation rate at high sound pressure levels (typically 10–30% at 1 kHz, for levels of 150–160 dB *re* $(20\ \mu\text{Pa})^2$) was at least of the right order of magnitude. It should be noted that the model used for calculating fibre drag is realistic only if the fibre spacing is larger than the viscous penetration depth δ, and this prevents its application to the blanket in reference [3] at frequencies below 500 Hz; at this frequency, the ratio of the typical fibre spacing to δ is 0·8.

5. SUMMARY AND CONCLUSIONS

1. A two-dimensional non-linear viscous flow code has been used to calculate the unsteady drag on a transversely oscillating circular cylinder. For sinusoidal motion, the non-linear drag response is limited to odd harmonics of the driving frequency.
2. The oscillatory Reynolds number R, based on the peak velocity and the cylinder diameter, was varied between 0·01 and 10; in this range the flow remains laminar.
3. The computed force harmonics are presented in dimensionless form as a function of a dimensionless oscillation amplitude K and a dimensionless frequency S. As the amplitude parameter K is reduced with S held fixed, the fundamental component of the force converges to the linearized analytical solution (Appendix A) to better than 1 per cent.
4. As K is increased with S held fixed, higher order odd harmonics appear in the drag force, and the fundamental amplitude departs from its linear value. The effect on the fundamental reaches about 1 per cent once K^2S exceeds 1; details are given in Figure 5.
5. Quasi-steady drag behaviour is approached as S is reduced, for a fixed Reynolds number. The numerically computed fundamental component converges to within about 5 per cent of the quasi-steady approximation when the ratio K^2S $(= R^2/S)$ exceeds 10^4.

6. The conclusions summarized above are based on an incompressible-flow model. The validity of the model requires that both the Helmholtz number N and the peak Mach number, $M = KN$, be much less than 1. The peak Reynolds number, $R = KS$, is required to be of order 10 or less, in view of (2) above.
7. The non-linearity threshold $K^2S = 1$ corresponds to placing the cylinder in a plane progressive wave sound field incident normal to the axis, with sound pressure levels

$$\begin{aligned} L_p &= 133 + 10\log_{10} F, \quad \text{dB } re\ (20\ \mu\text{Pa})^2 \text{ (in air)}, \\ L_p &= 219 + 10\log_{10} F, \quad \text{dB } re\ 1\ \mu\text{Pa}^2 \text{ (in water)}, \end{aligned} \tag{17}$$

   where F is the frequency in kHz.
8. In view of conclusion (7), the audio-frequency absorptive properties of air-filled fibrous materials should begin to be affected by non-linearity at sound pressure levels of around 140 dB. For quantitative predictions, based on preliminary results from the present model, see reference [13].
9. When a long cylinder is placed in a single-frequency plane progressive wave field, use of the quasi-steady approximation to calculate the force on the fluid at the driving frequency is not valid at low sound pressure levels. The approximation is valid only in the strongly non-linear regime corresponding to $K^2S = \rho v_{max}^2/\omega\mu = 10^3$–$10^4$, i.e., at levels 30–40 dB higher than those given in equation (17).

ACKNOWLEDGMENTS

The authors thank Geraint Price FRS FREng, Chair of the School of Engineering Sciences (SES) at the University of Southampton, for his support and encouragement during this study. Thanks also to Tim Farrant of SES (current address: 2H Offshore Engineering Ltd, Woking), who contributed significantly to the code development and ran the earlier test cases.

REFERENCES

1. G. G. STOKES 1851 *Transactions of the Cambridge Philosophical Society Part II* **9**, 8–106. On the effect of the internal friction of fluids on the motion of pendulums.
2. J. T. STUART 1963 in *Laminar Boundary Layers* (L. Rosenhead, editor), pp. 390–393. Oxford, UK: Clarendon Press, Chapter VII. Unsteady boundary layers.
3. H. L. KUNTZ and D. T. BLACKSTOCK 1987 *Journal of the Acoustical Society of America* **81**, 1723–1731. Attenuation of intense sinusoidal waves in air-saturated, bulk porous materials.
4. D. A. NELSON and D. T. BLACKSTOCK 1990 in *Frontiers of Nonlinear Acoustics*: *Proceedings of the 12th International Symposium on Nonlinear Acoustics* (M. F. Hamilton and D. T. Blackstock, editors), 621–626. London: Elsevier Science Publishers. Harmonic generation, propagation and attenuation for finite-amplitude tones in an air-filled porous material.
5. R. L. PANTON 1995 *Incompressible Flow*. New York: John Wiley. Second edition, section 10.7.
6. R. AKHAVAN, R. D. KAMM and A. H. SHAPIRO 1991 *Journal of Fluid Mechanics* **225**, 395–422. An investigation of transition to turbulence in bounded oscillatory Stokes flows. Part 1. Experiments.
7. R. AKHAVAN, R. D. KAMM and A. H. SHAPIRO 1991 *Journal of Fluid Mechanics* **225**, 423–444. An investigation of transition to turbulence in bounded oscillatory Stokes flows. Part 2. Numerical simulations.
8. C.-Y. WANG 1968 *Journal of Fluid Mechanics* **32**, 55–68. On high-frequency oscillatory viscous flows.
9. J. HOLTSMARK, I. JOHNSEN, T. SIKKELAND and S. SKAVLEM 1954 *Journal of the Acoustical Society of America* **26**, 26–39. Boundary layer flow near a cylindrical obstacle in an oscillating, incompressible fluid.

10. W. G. PRICE and M. TAN 1991 in *Proceedings of the International Conference on the Dynamics of Marine Vehicles and Structures in Waves* (W. G. Price, P. Temarel and A. J. Keane, editors), 125–133. London/New York: Elsevier. The evaluation of steady fluid forces on single and multiple bodies in low speed flows using viscous boundary elements.
11. S. TOMOTIKA and T. AOI 1950 *Quarterly Journal of Mechanics* **3**, 140–161. The steady flow of viscous fluid past a sphere and circular cylinder at small Reynolds numbers.
12. S. TOMOTIKA and T. AOI 1951 *Quarterly Journal of Mechanics* **4**, 401–406. An expansion formula for the drag on a circular cylinder moving through a viscous fluid at small Reynolds numbers.
13. C. L. MORFEY 1999 in *Proceedings of the 6th International Congress on Sound and Vibration Lyngby, Denmark*, 5–8 July 1999. (F. Jacobsen, editor), Vol. 7, 3209–3214. Auburn, USA: International Institute of Acoustics and Vibration. Nonlinear sound propagation in fibrous sound-absorbing materials.
14. M. RAY 1936 *Zeitschrift für Angewandte Mathematik und Mechanik* **16**, 99–108. The vibration of an infinite elliptic cylinder in a viscous fluid.
15. S. S. CHEN, M. W. WAMBSGANSS and J. A. JENDRZEJCZYK 1976 *Journal of Applied Mechanics, Transactions of the American Society of Mechanical Engineers* (series A) **43**, 325–329. Added mass and damping of a vibrating rod in confined viscous fluids.
16. W. G. PRICE and M. TAN 1991 in *Proceedings of the 18th Symposium on Naval Hydrodynamics* (E. P. Rood, editor), 801–814.Washington, D.C.: National Academy Press. The calculation of fluid actions on manoeuvring arbitrary shaped submerged bodies using viscous boundary elements.
17. W. G. PRICE and M. TAN 1992 *Proceedings of the Royal Society of London* **A438**, 447–466. Fundamental viscous solutions or 'transient oseenlets' associated with a body manoeuvring in a viscous fluid.

APPENDIX A: LINEARIZED THEORY FOR UNSTEADY DRAG

Stokes [1] solved the linearized incompressible problem for arbitrary S in series form in 1851; a more accessible account, using modern cylinder function notation, is published in reference [2]. The Stokes solution (summarized below) was generalized by Ray [14] to cylinders of elliptic cross-section, oscillating parallel to either axis of the ellipse. It was also generalized by Chen *et al.* [15] to describe the drag on a transversely oscillating circular cylinder, surrounded by a fixed outer cylinder with a uniform fluid-filled gap.

When a cylinder oscillates in an unbounded viscous fluid, with transverse velocity $v(t) = \mathrm{Re}\{\hat{v}\mathrm{e}^{\mathrm{j}\omega t}\}$, it applies a time-dependent force to the fluid that can be calculated analytically in the limit $|\hat{v}| = v_{max} \to 0$. The force $f(t)$ per unit length is given by

$$\frac{f(t)}{\mu v_{max}} = \mathrm{Re}\{H_1 \mathrm{e}^{\mathrm{j}\omega t}\}, \tag{A1}$$

$$H_1 = \mathrm{j}\frac{\pi}{4}S + 4\pi z\left[\frac{\mathrm{J}_1(z) - \mathrm{j}\,\mathrm{Y}_1(z)}{\mathrm{J}_0(z) - \mathrm{j}\,\mathrm{Y}_0(z)}\right]. \tag{A2}$$

Here S is the dimensionless frequency defined in equation (2) of the main paper, and

$$z = \tfrac{1}{2}(-\mathrm{j}S)^{1/2} = \tfrac{1}{2}(1 - \mathrm{j})(\tfrac{1}{2}S)^{1/2}. \tag{A3}$$

In the high-frequency limit $S \to \infty$, the complex force amplitude H_1 is dominated by the first term in equation (A2), which corresponds to the inertial loading force. At the opposite extreme, as $S \to 0$, equation (A2) is represented asympotically by

$$H_1 \approx \mathrm{j}\frac{\pi}{4}S - \frac{4\pi}{\frac{1}{2}\ln S + \ln\frac{1}{4}\gamma + \mathrm{j}\frac{\pi}{4}} \quad (S \to 0), \tag{A4}$$

where $\ln\gamma$ is the Euler–Mascheroni constant: thus $\gamma = 1{\cdot}781072\ldots$.

APPENDIX B: NUMERICAL METHOD

The flow was started from rest by giving the cylinder a transverse velocity

$$v(t) = \begin{cases} 0 & t < 0; \\ v_{max} \cos \omega t & t \geqslant 0 \end{cases}. \tag{B1}$$

A two-dimensional time-marching code, based on the boundary element method (BEM), was used to calculate the unsteady flow field. The force on the cylinder was deduced at each step from the surface pressure and viscous-stress distributions. The numerical scheme is described in detail in reference [16]; a brief summary is as follows.

The Navier–Stokes equation for incompressible two-dimensional flow is first expressed as an integral equation for the fluid velocity vector **u**, with the linearized Oseen operator on the left-hand side and non-linear terms on the right. The time-domain Green function for this operator is derived in reference [17]. Convolution in time and the two space dimensions yields the solution for **u**, from which the pressure and viscous stresses can be determined. Numerical implementation as a boundary element method (BEM) requires a similar discretization process to that used in a singularity distribution panel method. Viscous panels are distributed over the surface of the body and into the fluid domain, where the non-linear terms are included by regarding them as volume-distributed sources in the equation.

In applying the BEM code to the oscillating cylinder problem, careful attention was paid to (1) computational speed and accuracy, and (2) agreement with available benchmarks. Benchmark comparisons are shown in sections 3.2 and 3.3 of the main paper; the steps taken to ensure the required accuracy at minimum computational cost are described below.

Computational accuracy requires, in principle, that the dimensionless time step $\Delta\tau$ should be small; the flow simulation should run for many cycles to establish a steady state; the BEM mesh should be fine enough to resolve all length scales of the unsteady flow; and the mesh should extend far enough from the cylinder to capture the contribution of the non-linear volume-distributed sources (fluid domain terms).

In order to address the first two points above, a series of numerical experiments was run for the test case $K = 10^3$, $S = 10^{-3}$ using an approximate version of the code (with the fluid domain terms removed). The number of points per cycle, $n_P = (\Delta\tau)^{-1}$, and the total number of cycles, n_C, were both varied systematically, and in each case the force-harmonic amplitudes were based on the final cycle of data. The aims were to find what combinations of (n_P, n_C) yielded convergence of the fifth-harmonic force amplitude to within 2 per cent of its limiting value; and to find which point on the resulting n_P versus n_C curve corresponded to the shortest run time. The fifth-harmonic amplitude was chosen as the criterion in order to focus on the non-linear drag response; the reference value for convergence was based on $(n_P = 432, n_C = 18)$. Note that symmetry requires the even force harmonics to be zero, provided the flow does not exhibit chaotic behaviour; no such behaviour was observed, and the calculated even harmonics were at the level of numerical noise.

Results from this preliminary study are shown in Figure B1. For each of the odd-harmonic amplitudes ($n = 1, 3, 5, 7$), percentage error contours are plotted in the (n_C, n_P) plane. Higher odd harmonics were too small to capture numerically with the precision available. Based on the criteria above, the optimum combination ($n_P = 144$, $n_C = 3$) was adopted for all the non-linear drag calculations presented in section 3 of the main paper.

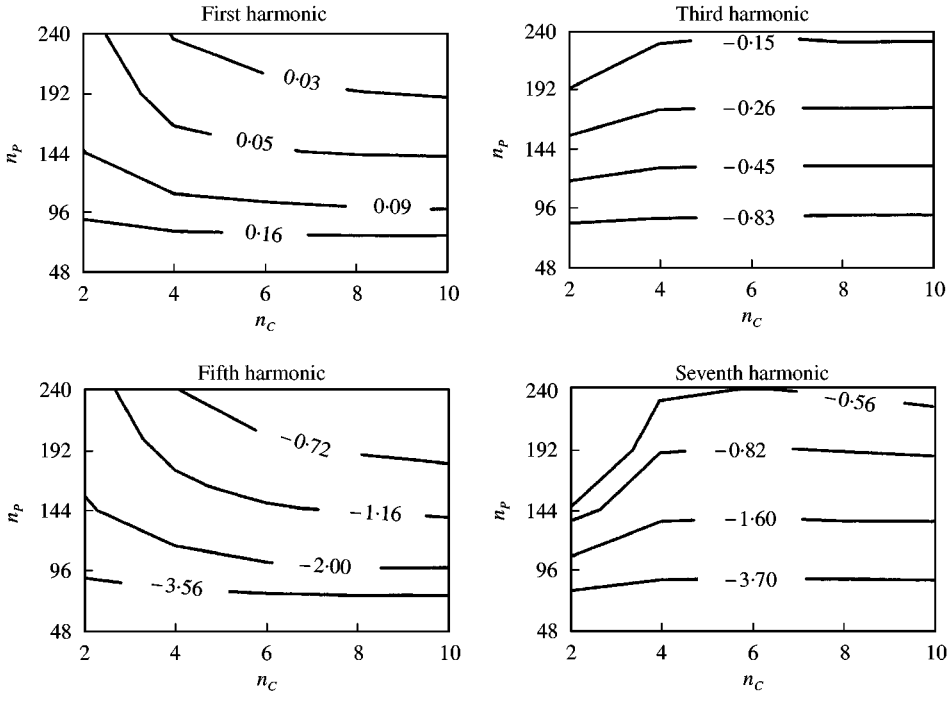

Figure B1. Percentage error contours in the n_P versus n_C plane, for the odd order force-harmonic amplitudes. All errors are relative to $n_P = 432$, $n_C = 18$.

APPENDIX C: LINEAR ACOUSTIC MODEL FOR PLANE WAVES IN A LIMP FLUID-SATURATED FIBRE BLANKET

The equations below are based on a Biot model in which the fluid pressure p and velocity u_f are spatially averaged values, associated with the macroscopic acoustic propagation mode in the two-phase medium (the characteristic wavelength is assumed large compared with the typical fibre spacing). The actual heat and momentum transfer rates from the skeleton to the fluid are represented by spatially smoothed source distributions applied to the fluid.

The sound field consists of single-frequency plane waves travelling in the x direction, with propagation factor $e^{j(\omega t - kx)}$; the complex wavenumber k is related to the phase speed v_{ph} and attenuation coefficient α by

$$k(\omega) = (\omega/v_{ph}) - j\alpha. \tag{C1}$$

Starting from the linearized equations for fluid momentum, entropy, and volume (continuity), the following dispersion and impedance relations may be derived for sound propagation in a limp porous material of porosity P close to unity ($1 - P = \phi \ll 1$):¶

$$\Gamma^2 = \left(\frac{P + \gamma\bar{y}_{eff}}{P + \bar{y}_{eff}}\right)\left(\frac{P + \bar{z}_{eff}}{P + D\bar{z}_{eff}}\right)\left(\frac{1}{1 + D\bar{z}_{eff}}\right), \qquad \Gamma = \frac{k(\omega)}{\omega/c_f}, \tag{C2}$$

¶These equations are corrected versions of the ones in reference [13]; the changes are of relative order ϕ and have been introduced so that equations (C2–C4) form a consistent $O(\phi)$ approximation. For the application in reference [13], the effect of the alterations is insignificant.

$$Z_{rel} = \frac{1}{P\Gamma}\left(1 - \frac{D}{\phi}\,\bar{z}_{eff}\right)^{-1}\left(\frac{P + \bar{z}_{eff}}{1 - D}\right), \qquad Z_{rel} = \frac{p}{\rho_f c_f (u_f - u_s)}. \tag{C3}$$

These yield the dimensionless complex wavenumber Γ and the dimensionless characteristic impedance Z_{rel}, for plane waves in the blanket. Symbol D denotes the ratio ρ_f/ρ_s. Subscripts f, s denote the fluid and solid components; ρ, c are density and sound speed; u_f is the spatially averaged fluid velocity, u_s is the fibre velocity, and p is the acoustic pressure. Quantities $\bar{y}_{eff}$, $\bar{z}_{eff}$ are normalized effective impedances (thermal and mechanical) for the solid skeleton, defined such that the heat and momentum transfer rates from the skeleton to the fluid per unit total volume of blanket are

$$Q = -\,\mathrm{j}\omega\rho_f C_{pf}\bar{y}_{eff}\,T_f \quad \text{and} \quad F = -\,\mathrm{j}\omega\rho_f\bar{z}_{eff}u_f - D\bar{z}_{eff}\frac{\partial p}{\partial x}. \tag{C4}$$

A sparse-array model of fluid–fibre interaction, summarized below in equations (C5–C7), is used to express the equivalent heat and momentum source terms in terms of acoustic variables. The effective impedances $\bar{y}_{eff}$ and $\bar{z}_{eff}$ in this model are given by

$$\bar{y}_{eff} = \phi\Big/\left(C - \frac{\pi x'^2}{y_f}\right), \qquad \bar{z}_{eff} = \phi\Big/\left(D - \frac{\pi x^2}{z_f}\right), \tag{C5}$$

where y_f and z_f are normalized impedances that give the heat and momentum transfer rates from an individual fibre; they are defined by $q = \kappa_f y_f(T_s - T_f)$ and $f = \mu_f z_f(u_s - u_f)$. Here q, f are the rates of heat and momentum transfer to the fluid per unit length of fibre, and T_s is the fibre surface temperature. For a single cylindrical fibre of infinite length and diameter d in an unbounded fluid, y_f and z_f are given by

$$y_f = 2\pi x' \mathrm{H}_1^{(2)}(x')/\mathrm{H}_0^{(2)}(x'), \qquad x' = \sqrt{-\tfrac{1}{4}\mathrm{j}S\mathrm{Pr}}, \tag{C6}$$

$$z_f = \pi[-x^2 + 4x\mathrm{H}_1^{(2)}(x)/\mathrm{H}_0^{(2)}(x)], \qquad x = \sqrt{-\tfrac{1}{4}\mathrm{j}S}. \tag{C7}$$

Here $\mathrm{H}_n^{(2)}$ is the outgoing-wave Hankel function, S is the Stokes number $\omega d^2/\nu_f$, and Pr is the Prandtl number $C_p\mu/\kappa$ of the fluid. Other symbols used above are C = thermal capacity ratio $(\rho C_p)_f/(\rho C_p)_s$, C_p = constant-pressure specific heat, γ = specific-heat ratio of fluid, κ = thermal conductivity.

Note that the use of C and D in equations (C2–C5) is a simplification, based on neglecting variations in temperature through each fibre, and treating the skeleton as limp. Also, compression of the fibre material has been neglected in deriving equations (C2, C3). To allow for transverse temperature gradients in a cylindrical fibre, C is replaced by

$$C' = \tfrac{1}{2}\beta[\mathrm{J}_0(\beta)/\mathrm{J}_1(\beta)]C, \qquad \beta = \tfrac{1}{2}d\sqrt{-\mathrm{j}\omega\rho_s C_{ps}/\kappa_s}. \tag{C8}$$

To allow for finite skeleton stiffness, D is replaced by

$$D' = D/(1 - \Gamma^2 V^2), \qquad V = c_{skel}/c_f; \tag{C9}$$

here c_{skel} is the *in vacuo* longitudinal wave speed of the skeleton.

APPENDIX: NOMENCLATURE

C_D	drag coefficient of cylinder
c	sound speed of fluid
d	diameter of cylinder
$f(t)$	force applied to fluid per unit length of cylinder
H_n	complex dimensionless harmonic amplitude
h_n	dimensionless magnitude $\lvert H_n \rvert$
j	$\sqrt{-1}$
K	oscillation amplitude parameter, equation (8)
L_p	sound pressure level
M	Mach number v_{max}/c
N	Helmholtz number $\omega d/c$
n	harmonic number
P	porosity
R	oscillatory Reynolds number, equation (1)
R_{mean}	steady flow Reynolds number
S	frequency parameter, equation (2)
t	time
$\mathbf{U}$	fluid velocity at infinity
$\mathbf{u}(\mathbf{x}, t)$	fluid velocity field
$\mathbf{V}$	rigid-body velocity
$v(t)$	oscillatory cylinder velocity in stationary fluid
v_{ph}	phase speed
α	attenuation coefficient
γ	1·781 072 …
ε_1	$\lvert h_1 - h_a \rvert / h_a$
δ	viscous penetration depth, $\sqrt{2\nu/\omega}$
ξ	cylinder displacement
λ	acoustic wavelength
μ	viscosity of fluid
ν	kinematic viscosity, μ/ρ
ρ	fluid density
σ	$R_{mean}/4$
τ	dimensionless time measured in cycles
ϕ	volume fraction $(1 - P)$ occupied by fibres; arbitrary function
ω	angular frequency

Subscripts

a	analytical value given by linearized theory
max	peak value of oscillatory quantity
n	harmonic order
∞	value in far field